

# A modified Embedded-Atom Method interatomic potential for uranium-silicide

Benjamin Beeler<sup>a,\*</sup>, Michael Baskes<sup>b,c,d</sup>, David Andersson<sup>b</sup>, Yongfeng Zhang<sup>a</sup>

<sup>a</sup>*Idaho National Laboratory, Idaho Falls, ID 83415*

<sup>b</sup>*Los Alamos National Laboratory, Los Alamos, NM 87545*

<sup>c</sup>*University of California-San Diego, San Diego, CA 92093*

<sup>d</sup>*Mississippi State University, MS 39762*

---

## Abstract

Uranium-silicide (U-Si) fuels are being pursued as a possible accident tolerant fuel (ATF). This uranium alloy fuel benefits from higher thermal conductivity and higher fissile density compared to UO<sub>2</sub>. In order to perform engineering scale nuclear fuel performance simulations, the material properties of the fuel must be known. Currently, the experimental data available for U-Si fuels is rather limited. Thus, multiscale modeling efforts are underway to address this gap in knowledge. In this study, a semi-empirical modified Embedded-Atom Method (MEAM) potential is presented for the description of the U-Si system. The potential is fitted to the formation energy and structural properties of U<sub>3</sub>Si<sub>2</sub>. The primary phase of interest (U<sub>3</sub>Si<sub>2</sub>) is accurately described over a wide temperature range and displays good behavior under irradiation and with free surfaces. The potential can also describe a variety of U-Si phases across the composition spectrum.

---

## 1. Introduction

Nuclear fuels operate in reactor environments experiencing high temperatures, temperature gradients and mechanical stress under neutron irradiation. This complex and extreme environment, combined with the high power density that allows nuclear fuels to be economical, presents safety challenges during off-normal events and accidents. In addition to innovations in reactor design, research is focused on the development of advanced materials [1] to improve accident tolerance. Accident-tolerant fuel (ATF) [2] is being considered as a potential fuel type for future and existing light-water reactors (LWRs). ATF's aim to provide additional coping time in the event of an accident (such as a loss of coolant accident) due to the inherent properties of the fuel, while maintaining good operational characteristics. Uranium-Silicide (U-Si), and particularly U<sub>3</sub>Si<sub>2</sub>, is being considered as a fuel candidate in ATFs. U<sub>3</sub>Si<sub>2</sub> exhibits both higher uranium density than traditional UO<sub>2</sub> LWR fuel, thus allowing for the possibility of reduced enrichments, fewer assemblies and/or an extended lifetime in the core. U<sub>3</sub>Si<sub>2</sub> also possesses a higher thermal conductivity than UO<sub>2</sub>, allowing for a lower fuel centerline temperature and more rapid heat removal during off-normal conditions.

---

\*Corresponding author

Email address: [benjamin.beeler@inl.gov](mailto:benjamin.beeler@inl.gov) (Benjamin Beeler)

In order for the implementation of  $\text{U}_3\text{Si}_2$  to become a reality, the scientific community must be able to perform continuum scale descriptive and predictive nuclear fuel performance simulations. To perform such simulations, the material properties of the fuel must be known. Subjecting  $\text{U}_3\text{Si}_2$  to the in-reactor environment leads to microstructural changes due to the evolution of radiation produced defects, segregation and precipitation of fission products, and mechanical deformation. These changes in fuel microstructure change fuel properties, directly impacting fuel performance and safety. The ability to understand and model microstructural changes throughout the lifetime of the fuel is critical in developing fuel performance modeling codes. However, the current experimental data available for U-Si fuels is rather limited. This includes crystal structures [3, 4], phase diagrams [5], thermal conductivity, heat capacity, thermal expansion [6, 7], high pressure diffraction [8], formation enthalpies [9, 10, 11, 12, 13] and irradiation studies [7, 14]. Thus, multiscale modeling efforts are underway to address this gap in knowledge.

One recent investigation involved first principles calculations characterizing a variety of properties in the U-Si system [15]. These calculations have been able to provide insight where experimental information is lacking. However, first principles calculations are limited in their ability to investigate systems larger than a few hundred atoms in size, and are severely restricted in their ability to investigate properties at non-zero temperatures. Thus, although these types of investigations are of critical importance, branching to higher time and length scales is necessary for the investigation of larger, more complex systems. Molecular dynamics-density functional theory (MD-DFT) can be employed to look at non-zero temperatures, but are still restricted to a very small system size and very short time scale. In order to overcome this limitation, interatomic potentials can be employed within molecular dynamics (MD) methods to solve Newton's equations of motion. In this way, MD can be used to calculate relevant properties above 0 K on a nanosecond time and nanometer spatial scale. Information obtained from molecular statics and dynamics simulations can then be input into higher level modeling methodologies such as phase field, kinetic Monte Carlo or continuum level finite element modeling. In this manner, physics-based multiscale microstructural evolution models can be generated. Thus, development of an interatomic potential to describe the U-Si system is a critical step in branching time and length scales with the long-term goal of developing a descriptive and predictive nuclear fuel performance code.

Very few interatomic potentials have been constructed for uranium-based alloys. This is due to the inherent difficulty in describing the behavior of f-electrons and the mechanical instability of the  $\gamma$  phase of uranium at low temperatures. Several interatomic potentials have been developed for pure uranium [16, 17, 18, 19, 20, 21], with only a few being adapted into alloy potentials for U-Zr [22], U-Al [23] and U-Mo [24]. Based on the functionality of the modified Embedded-Atom Method (MEAM) variants of U and U-Zr [16, 22] as well as their inclusion of fission gases Xe, Kr and He [17], it is determined that this is a suitable potential form to pursue in attempting to describe the U-Si system.

This manuscript presents a MEAM interatomic potential for the description of the U-Si system, with particular emphasis on  $\text{U}_3\text{Si}_2$ . No interatomic potentials for the U-Si system have been constructed prior to

this work.

## 2. MEAM Theory

The Embedded-Atom Method (EAM) [25, 26, 27] has been shown to predict the properties of alloys and metals quite well. The EAM is the most widely used semi-empirical potential, with applications including calculations of point defects [28], melting [29], grain boundary structure and energy [30], dislocations [31] [40], segregation [32], fracture [33] and surface structure [34]. The basis of the EAM is that the cohesive energy can be expressed in terms of embedding energies. In this view, each atom in the metal is embedded into the electron gas created by the other atoms. The EAM provides a robust means of calculating structure and energetics; however, it is best suited strictly for purely metallic systems with no directional bonding. From the EAM, the total energy of a system of atoms is given by equation 1:

$$E = \sum_i \{F(\bar{\rho}_i) + \frac{1}{2} \sum_{j \neq i} S_{ij} \phi(R_{ij})\} \quad (1)$$

where  $i$  and  $j$  are the individual atoms of the model [27, 25]. The pair interaction between atoms  $i$  and  $j$  is given by  $\phi$  [35] and is dependent on the separation between the atoms  $R_{ij}$ .

$$\phi(R) = \frac{2}{Z} \left\{ E^u(R) - F\left(\frac{\bar{\rho}^0(R)}{Z}\right) \right\} \quad (2)$$

In equation 2,  $Z$  is the number of first neighbors,  $\bar{\rho}^0(R)$  is the background electron density and  $\{E^u(R)\}$  is the per atom energy of the reference structure as a function of nearest-neighbor distance  $R$  [36] obtained from the universal equation of state of Rose et al. [34] given in equation 3.

$$E^u(R) = -E_c(1 + a^* + \delta \times (\frac{r_e}{r}) \times (a^*)^3)e^{(-a^*)} \quad (3)$$

with

$$a^* = \alpha(\frac{R}{r_e} - 1) \quad (4)$$

and

$$\alpha^2 = \frac{9\omega B}{E_c} \quad (5)$$

where  $E_c$ ,  $r_e$ ,  $\omega$  and  $B$  are the cohesive energy, nearest neighbor distance, atomic volume and bulk modulus, respectively, evaluated at equilibrium in the reference structure. The background electron density is given by:

$$\bar{\rho}^0(R) = Z\rho^{a(0)}(R) \quad (6)$$

where  $\rho^{a(0)}$  is an atomic electron density discussed below. The embedding function,  $F$ , is given in equation 7 and is the energy required to embed atom  $i$  into a system with a background electron density  $\bar{\rho}_i$ .

$$F(\bar{\rho}) = AE_c \frac{\bar{\rho}}{Z} \ln \frac{\bar{\rho}}{Z} \quad (7)$$

The modification to the EAM is a function of how the electron density at a certain point,  $\rho_i$ , is calculated. In the traditional EAM,  $\rho_i$  is simply the linear supposition of spherically averaged atomic electron densities:

$$\rho_i^{(0)} = \sum_{j \neq i} \rho_j^{a(0)}(R_{ij}) \quad (8)$$

whereas the MEAM introduces angularly dependent terms to augment  $\bar{\rho}_i$  as shown in equation 9 through equation 11 [36, 37].

$$(\rho_i^{(1)})^2 = \sum_{\alpha} \left\{ \sum_{j \neq i} x_{ij}^{\alpha} \rho_j^{a(1)}(R_{ij}) \right\}^2 = \sum_{j, k \neq i} \rho_j^{a(1)}(R_{ij}) \rho_k^{a(1)}(R_{ik}) \cos\{\theta_{ijk}\} \quad (9)$$

$$(\rho_i^{(2)})^2 = \sum_{\alpha, \beta} \left\{ \sum_{j \neq i} x_{ij}^{\alpha} x_{ij}^{\beta} \rho_j^{a(2)}(R_{ij}) \right\}^2 - \frac{1}{3} \sum_{j \neq i} [\rho_j^{a(2)}(R_{ij})]^2 \quad (10)$$

$$(\rho_i^{(3)})^2 = \sum_{\alpha, \beta, \gamma} \left\{ \sum_{j \neq i} x_{ij}^{\alpha} x_{ij}^{\beta} x_{ij}^{\gamma} \rho_j^{a(3)}(R_{ij}) \right\}^2 - \frac{3}{5} \sum_{j \neq i} [\rho_j^{a(3)}(R_{ij})]^2 \quad (11)$$

Here, the  $\rho^{a(l)}$  are the atomic densities which represent the decrease in the contribution with distance  $R_{ij}$  and the  $\alpha, \beta, \gamma$  summations are each over the three coordinate directions with  $x_{ij}^{\alpha}$  being the distance the ratio  $R_{ij}^{\alpha}/R_{ij}$  with  $R_{ij}^{\alpha}$  being the  $\alpha$  component of the distance vector between atoms  $i$  and  $j$  [29]. Similar to equation 9, equations 10 and 11 can be put in a form that has a dependence on the angle between atoms  $i, j$  and  $k$  ( $\theta_{ijk}$ ), and this has been done by Baskes et al. [38]. Atomic electron densities are assumed to decrease exponentially,

$$\rho_i^{a(l)}(R) = e^{[-\beta^{(l)}(\frac{R}{r_e} - 1)]} \quad (12)$$

where  $\beta^{(l)}$  are the decay lengths. To obtain the background electron density from the partial electron densities we make the assumption that the angular terms are a small correction to the EAM.

$$(\rho_i^{(0)})^2 = \sum_{l=0}^3 \bar{t}_i^{(l)} (\rho_i^{(l)})^2 \quad (13)$$

where the  $\bar{t}_i^{(l)}$  [39] are combinations of model constants  $t^l$  that are associated with the atom types of neighbors  $i$ .

Many body screening is implemented through a screening function,  $S_{ij}$ , that quantifies screening between two atoms i and j due to other atoms in the system, k. The atomic electron densities and the pair potential are multiplied by this function. The screening function depends on all other atoms in the system:

$$S_{ij} = \prod_{k \neq i,j} S_{ijk} \quad (14)$$

where  $S_{ijk}$  is calculated using a simple geometric construction. The screening factor  $S_{ijk}$  is defined as:

$$S_{ijk} = f_c \left[ \frac{C - C_{min}}{C_{max} - C_{min}} \right] \quad (15)$$

where C is a geometric parameter, and  $C_{min}$  and  $C_{max}$  are limiting values of C. The smooth cutoff function is:

$$f_c(x) = \begin{cases} 1 & x \geq 1 \\ [1 - (1 - x)^6]^2 & 0 < x < 1 \\ 0 & x \leq 0 \end{cases} \quad (16)$$

A radial cutoff function is also applied to the atomic electron densities and pair potential which is given by  $f_c[(r_c - r)/\lambda]$  where  $r_c$  is the cutoff distance of 6 Å and  $\lambda$  gives the cutoff region and was chosen to be 0.1. The MEAM has been shown to accurately predict the behavior of complex systems such as plutonium [36] and tin [40]. It should be noted that these equations are for a single component system and can be generalized for a multicomponent system, as was done in [41].

### 3. Fitting Procedure

In order to create a functional uranium-silicide (U-Si) binary interatomic potential, there must first exist (or be generated) suitable potentials for each individual element. A uranium potential from Moore, *et al.* [22] is utilized in the fitting. This MEAM interatomic potential performs excellently in describing the body-centered cubic phase of uranium and the alloy behavior of UZr. For the Si MEAM contribution, the initial potential utilized was from Baskes [35]. Upon finding this potential over-predicted the Si-Si dimer distance (compared to the reference value of 2.25 Å[42]), the fitting of a new Si-Si potential was undertaken in an attempt to rectify this discrepancy, as well as increasing the vacancy formation energy in diamond cubic silicon. The only MEAM parameters allowed to vary in the Si potential fitting process were  $\beta^0$ ,  $\beta^1$ ,  $\beta^2$ ,  $\beta^3$ ,  $t^1$ ,  $C_{min}$  and  $C_{max}$ . The resulting potential is shown in table 1, with the associated properties of the original and new MEAM potentials shown in table 2. Although the Si-Si dimer distance was unchanged, the formation energy of a vacancy in diamond Si is increased. All other properties are relatively unaffected.

The fitting procedure to develop cross-species parameters (U-Si interactions) involves a reference phase ( $L1_2$ -U<sub>3</sub>Si), a starting guess for MEAM parameters, and is then refined via a script that gives a random step to all relevant MEAM parameters. This updated potential is then input into LAMMPS [43] and a

Table 1: Silicon MEAM potential parameters

| Parameter  | Original Si-MEAM | New Si-MEAM |
|------------|------------------|-------------|
| attrac     | 0                | 0           |
| repuls     | 0                | 0           |
| alpha      | 4.87             | 4.87        |
| $\beta^0$  | 4.4              | 4.4662      |
| $\beta^1$  | 5.5              | 9.4016      |
| $\beta^2$  | 5.5              | 13.3826     |
| $\beta^3$  | 8.5              | 8.6993      |
| alat (Å)   | 5.431            | 5.431       |
| $E_c$ (eV) | 4.63             | 4.63        |
| A          | 1                | 1           |
| $t^0$      | 1                | 1           |
| $t^1$      | 2.05             | 2.8841      |
| $t^2$      | 4.47             | 4.47        |
| $t^3$      | -1.80            | -1.80       |
| $C_{min}$  | 2.0              | 1.7215      |
| $C_{max}$  | 2.8              | 2.4942      |

series of simulations are performed, the output of which is utilized to calculate a weighted-error summation. The script then either accepts or rejects the prescribed changes to the MEAM parameters based on the reduction of the total weighted-error. The emphasis of the fitting procedure was the  $U_3Si_2$  phase, which possesses a relatively complex crystal structure, with a 10 atom unit cell in space group  $P4/mbm$ -No. 127, two unique uranium atomic sites (2a (0, 0, 0) and 4h (0.181, 0.681, 0.5) ) and one unique silicon atomic site (4g (0.389, 0.889, 0) ), as first reported by Zachariasen [3]. The cohesive energy, lattice constants and elastic constants of the  $U_3Si_2$  phase were given priority with respect to the error weighting, and are thus considered the primary fitting targets. Additionally, a number of alternative structures were discovered throughout the fitting procedure via a heating and quenching simulation. Up to four alternative structures were included as fitting targets at a given time, enforcing the condition that these structures exhibited a higher energy than the experimental structure. A variety of other simulations were performed periodically to serve as sanity checks for the potential, the entirety of which is beyond the scope of this paper. The potential parameters are shown in table 3. Screening parameters are given in LAMMPS format (i.e.,  $C_{max}(I,J,K)$  is a screening parameter when I-J pair is screened by K, where I, J and K are atom types).

For the sake of clarity and reproducibility, LAMMPS MEAM-specific parameters are included in table 4. It should also be noted that a non-standard implementation of MEAM within LAMMPS (which relates

Table 2: Properties of silicon MEAM potentials. Units are as follows: E (eV/atom), a ( $\text{\AA}$ ),  $c_{xx}$  (GPa),  $E_{form}$  (eV).

| Structure | Property         | Original Si-MEAM | New Si-MEAM |
|-----------|------------------|------------------|-------------|
| Diamond   | E                | -4.63            | -4.63       |
|           | a                | 5.431            | 5.431       |
|           | $c_{11}$         | 163.8            | 165.2       |
|           | $c_{12}$         | 64.6             | 64.6        |
|           | $c_{44}$         | 78.8             | 95.2        |
|           | $E_{form}^{vac}$ | 3.858            | 4.142       |
| FCC       | E                | -4.065           | -4.151      |
|           | a                | 4.100            | 4.098       |
| HCP       | E                | -4.067           | -4.152      |
|           | a                | 2.904            | 2.902       |
|           | c/a              | 1.624            | 1.624       |
| SC        | E                | -4.337           | -4.358      |
|           | a                | 2.622            | 2.622       |
| BCC       | E                | -4.316           | -4.286      |
|           | a                | 3.145            | 3.176       |
| Dimer     | E                | -2.558           | -2.546      |
|           | a                | 2.431            | 2.443       |

to modification of the smooth cutoff function) was utilized for the existing U MEAM potential and this subsequent U-Si potential. Please contact the authors to obtain the required modifications in order to accurately utilize the potential.

Table 3: Uranium-silicon MEAM potential parameters. Uranium is atom type 1 and silicon is atom type 2.

| Parameter              | U-Si MEAM |
|------------------------|-----------|
| $E_c$ (eV)             | 5.36      |
| $r_e$ ( $\text{\AA}$ ) | 3.05      |
| lattce                 | 112       |
| $r_c$ ( $\text{\AA}$ ) | 6.0       |
| attrac                 | 0.1873    |
| repuls                 | 0.0742    |
| alpha(1,2)             | 4.978     |
| rho(2)                 | 4.151     |
| rho(1)                 | 1         |
| $C_{min}(1,1,2)$       | 0.124     |
| $C_{max}(1,1,2)$       | 2.604     |
| $C_{min}(1,2,1)$       | 2.107     |
| $C_{max}(1,2,1)$       | 2.741     |
| $C_{min}(1,2,2)$       | 1.549     |
| $C_{max}(1,2,2)$       | 2.517     |
| $C_{min}(2,2,1)$       | 0.985     |
| $C_{max}(2,2,1)$       | 1.606     |

Table 4: LAMMPS MEAM-specific parameters [43].

| Parameter             | U-Si MEAM |
|-----------------------|-----------|
| bkgd_dyn              | 1         |
| nn2                   | 1         |
| delr ( $\text{\AA}$ ) | 0.1       |
| ialloy                | 1         |
| augt1                 | 0         |
| emb_lin_neg           | 1         |

#### 4. U-Si MEAM Potential Results

The results for fundamental properties of  $\text{U}_3\text{Si}_2$  at 0 K are displayed in table 5 and compared to experiments [3, 13] and DFT calculations [15] (DFT+U results from [15] are used for comparison but simply referred to as DFT here). The formation energy and the volume per atom are very accurate. The  $a$  lattice constant is slightly underestimated and the  $c$  lattice constant is slightly overestimated. The elastic constants show varying degrees of agreement with DFT predictions. Excellent agreement shown for  $G^{xy}$  and  $G^{xz}$  (equations 17 and 18), but significant variance is observed for  $C_{44}$ , for example. The resulting bulk modulus, calculated via the elastic constants in equation 19, is overestimated. The bulk modulus was also calculated via the Birch-Murnaghan curve [44, 45], yielding a value of 114 GPa, which is consistent with the calculation of the bulk modulus via elastic constants. A comparison of the elastic constants predicted by MEAM and calculated via DFT are displayed in Figure 1. The blue line represents a 1:1 agreement between MEAM and DFT. It is observed a general overstiffness prediction of the elastic constants, with the exception being  $C_{44}$ , which is underpredicted. The root-mean-square error over the nine calculated elastic constants is 35.4 GPa.

$$G^{xy} = \frac{\frac{C_{11} + C_{22}}{2} - C_{12}}{2} \quad (17)$$

$$G^{xz} = \frac{\frac{C_{11} + C_{33}}{2} - C_{13}}{2} \quad (18)$$

$$B = (C_{11} + C_{22} + C_{33} + 2 * C_{12} + 2 * C_{13} + 2 * C_{23}) / 9 \quad (19)$$

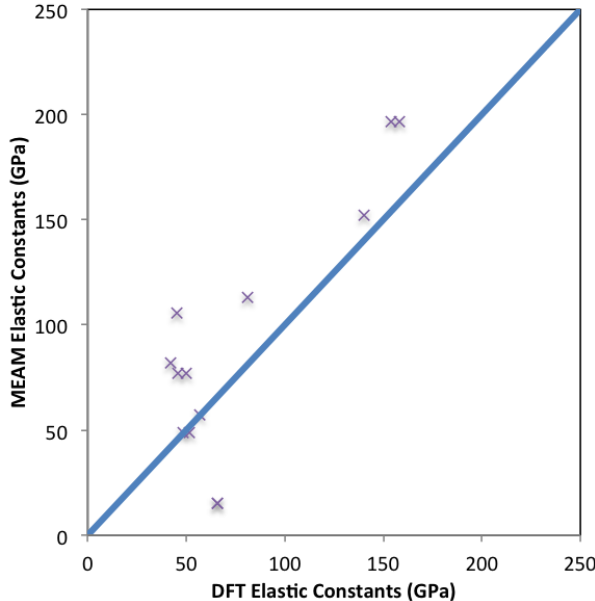


Figure 1: Comparison of  $\text{U}_3\text{Si}_2$  elastic constants as calculated by DFT and MEAM.

Table 5: Properties of  $\text{U}_3\text{Si}_2$  at 0 K. Results from the MEAM U-Si potential are compared to experiments<sup>1</sup>[3]<sup>2</sup>[13] and DFT<sup>3</sup>[15] calculations. Units are as follows: E (eV/atom), V/at ( $\text{\AA}^3/\text{atom}$ ), a and c ( $\text{\AA}$ ),  $C_{xx}$ , B and G (GPa).

|          | Reference           | U-Si MEAM |
|----------|---------------------|-----------|
| E        | -0.356 <sup>2</sup> | -0.354    |
| V/at     | 20.844 <sup>1</sup> | 20.950    |
| a        | 7.32 <sup>1</sup>   | 7.157     |
| c        | 3.89 <sup>1</sup>   | 4.090     |
| c/a      | 0.531 <sup>1</sup>  | 0.572     |
| $C_{11}$ | 149 <sup>3</sup>    | 196.6     |
| $C_{33}$ | 139 <sup>3</sup>    | 152.3     |
| $C_{12}$ | 49 <sup>3</sup>     | 81.9      |
| $C_{13}$ | 48 <sup>3</sup>     | 77.0      |
| $C_{44}$ | 63 <sup>3</sup>     | 15.3      |
| $C_{66}$ | 46 <sup>3</sup>     | 105.8     |
| B        | 81 <sup>3</sup>     | 113       |
| $G^{xy}$ | 50 <sup>3</sup>     | 57        |
| $G^{xz}$ | 48 <sup>3</sup>     | 49        |

The  $\text{U}_3\text{Si}_2$  structure is shown in figure 2 [3]. This figure illustrates a supercell of  $2 \times 2 \times 3$  unit cells with periodic boundaries. In comparing the experimental structure to the predicted structure from the MEAM potential, a slight expansion of uranium atoms (red) in the purely uranium plane is observed. Also, a minuscule clockwise rotation of atoms in the unit cell with respect to the experimental structure is observed. This alteration is nearly imperceptible, except by analyzing the radial distribution functions (RDFs), as shown in figure 3. The RDF shows that the structure is not capturing the smallest interatomic distance; this is due to the slight expansion in the U plane and the clockwise rotation of U and Si atoms. These minor distortions slightly increase the first nearest neighbor distance by approximately 0.2  $\text{\AA}$  and slightly decrease the second and third nearest neighbor distances, as shown in Figure 3 in the distance regime of 2.8-3  $\text{\AA}$ . The first nearest-neighbor distance is a Si-Si distance. It is possible this is overestimated due to the inherent properties of the Si MEAM potential, which over-predicts the Si-Si dimer distance.

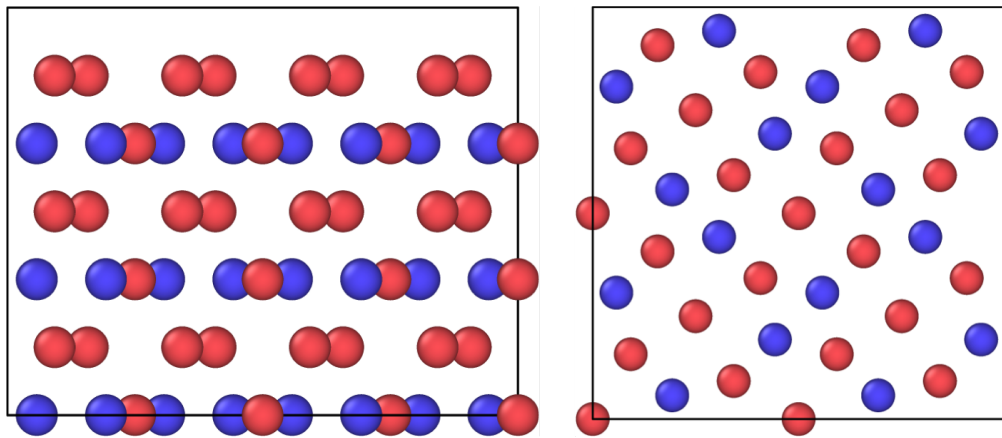


Figure 2: (100) view (left) and (001) view (right) of the experimental structure of  $\text{U}_3\text{Si}_2$ . Uranium atoms in red; Silicon atoms in blue.

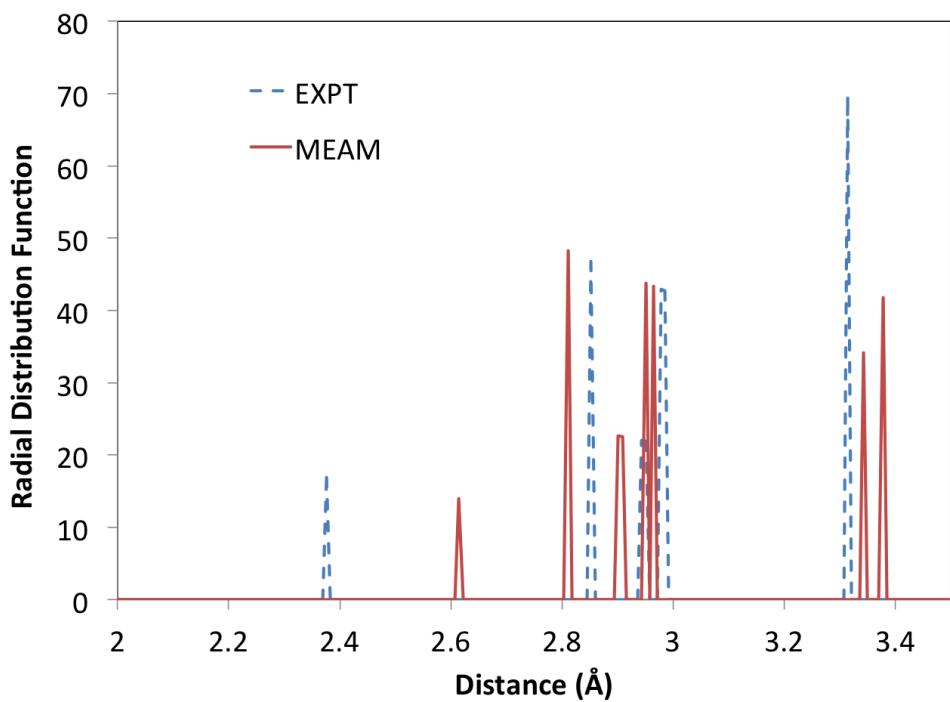


Figure 3: Radial distribution functions of  $\text{U}_3\text{Si}_2$ , comparing the MEAM predicted structure with the experimental structure.

Moving beyond the perfect crystal, the next step in testing the accuracy of the potential is to investigate point defects. Single point defects (vacancy, interstitial, antisite) were considered as a means of accommodating a change in stoichiometry. The methodology for calculating point defect energetics is outlined in [46]. Point defect energies for the  $\text{U}_3\text{Si}_2$  system are shown in table 6 and compared to results from DFT [46]. Bound Schottky defects are also shown in table 6. There exist two unique uranium sites in the  $\text{U}_3\text{Si}_2$  structure. Both U sites are investigated and denoted simply U1 (for the 2a site) or U2 (for the 4h site), as in Remschnig, *et al.* [4]. Three interstitial sites were investigated, as in [46], but only the lowest energy interstitial is reported in table 6. The bound Schottky defect consists of two U2 vacancies, one U1 vacancy and two Si vacancies, such that crystallographic accuracy is maintained, as well as the accurate chemical formula. Excellent agreement is observed for the formation energy of the U1 vacancy site and the Si interstitial. Reasonable agreement is observed for the U2 vacancy and all anti-site defects. The uranium interstitial energy is substantially overestimated. The Si vacancy formation energy is substantially underestimated, and this likely leads to the bound Schottky defect energy being substantially underestimated as well.

Table 6: Properties of point defects in  $\text{U}_3\text{Si}_2$  at 0 K. Results from the MEAM U-Si potential are compared to DFT calculations [46]. Units are eV.

|                | U-Si MEAM | DFT  |
|----------------|-----------|------|
| U1 vac         | 0.65      | 0.68 |
| U2 vac         | 0.90      | 1.20 |
| Si vac         | 0.57      | 1.59 |
| U int          | 2.22      | 0.76 |
| Si int         | 0.13      | 0.19 |
| U1 anti        | 0.25      | 0.16 |
| U2 anti        | 0.25      | 0.35 |
| Si anti        | 0.34      | 0.35 |
| Schottky Bound | 5.21      | 7.57 |

In order to ensure that the potential is not restricted to studying only the  $\text{U}_3\text{Si}_2$  phase, other phases, experimental and theoretical, were examined that were not included in the fitting procedure. These include the FeB-USi, B1-USi, AlB<sub>2</sub>-USi<sub>2</sub>, L1<sub>2</sub>-USi<sub>3</sub>,  $\text{U}_3\text{Si}_5$  phases and the L1<sub>2</sub>,  $\alpha$  and  $\beta$  phases of  $\text{U}_3\text{Si}$ . The results are shown in Figures 4 and 5 as the formation energy as a function of uranium concentration and the volume per atom as a function of uranium concentration, respectively. In Figure 4, excellent agreement is observed for the uranium rich portion of the composition range. For  $\text{U}_3\text{Si}$ ,  $\text{U}_3\text{Si}_2$  and FeB-USi, formation energies are nearly identical to those from experiments [13], and DFT calculations [15]. Also, the minimum is observed at USi<sub>2</sub> for the MEAM potential, which matches experiment, and the minimum is observed at  $\text{U}_3\text{Si}_5$  (a distorted USi<sub>2</sub> structure with  $\frac{1}{6}$  of the silicon sites vacant) for DFT, which shows reasonable agreement.

The energy of  $\text{USi}_2$  is slightly lower than what would be consistent with the convex hull behavior shown in experiments [13]. Significant variance is observed for the  $\text{USi}_3$  and B1-USi structures. These structures are deemed to be of less importance as they are either far away from the composition range of interest, in the case of  $\text{USi}_3$ , or not the low energy structure, in the case of B1-USi. In Figure 5, there exists a general negative parabolic trend in the volume predicted via the USi MEAM potential as a function of composition. This matches the trends from DFT quite well, with the exception being MEAM overestimating the volume per atom of the FeB-USi structure. Per-atom volumes of  $\text{U}_3\text{Si}_2$  and  $\text{U}_3\text{Si}$  agree very well. Given that only  $\text{U}_3\text{Si}_2$  was utilized as a fitting target and  $\text{L1}_2\text{-}\text{U}_3\text{Si}$  was utilized as a reference structure, there is considerable agreement across the entire composition spectrum when comparing MEAM predicted results to the results from DFT calculations. It should be noted that DFT (GGA without Hubbard U) calculations [15] found the presence of another structure for  $\text{U}_3\text{Si}_2$  that is lower in energy than the experimental structure. This structure was destabilized by the addition of the Hubbard U term, which resulted in the correct prediction of the experimental structure as the ground state. In order to ensure no such low energy structure exists in the MEAM potential energy landscape, this alternate  $\text{U}_3\text{Si}_2$  structure was analyzed and found to be 0.125 eV/atom higher in energy than the experimental structure. Thus, the MEAM interatomic potential is predicting the experimental structure to be the equilibrium phase, which is encouraging.

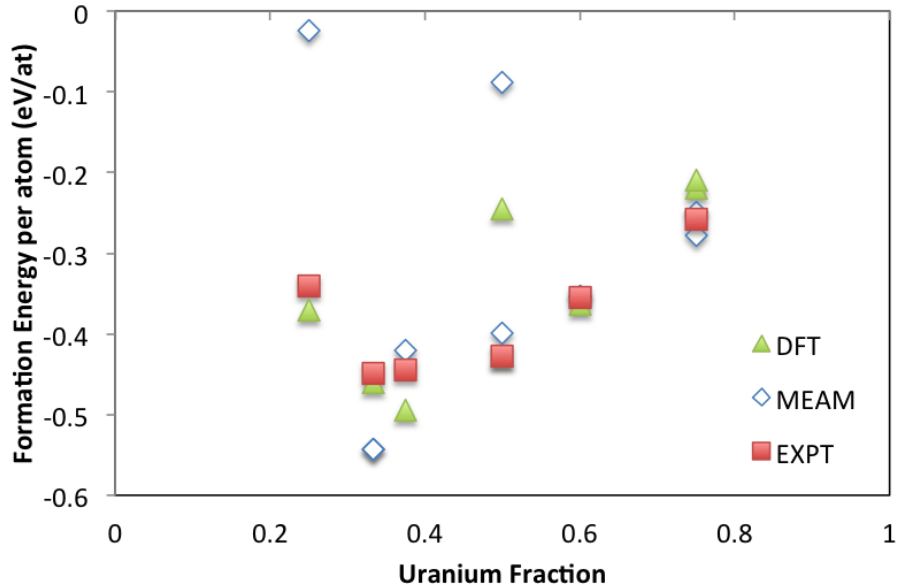


Figure 4: Formation energy per atom as a function of uranium concentration for a variety of phases in the U-Si system compared to DFT calculations [15] and experiments [13].

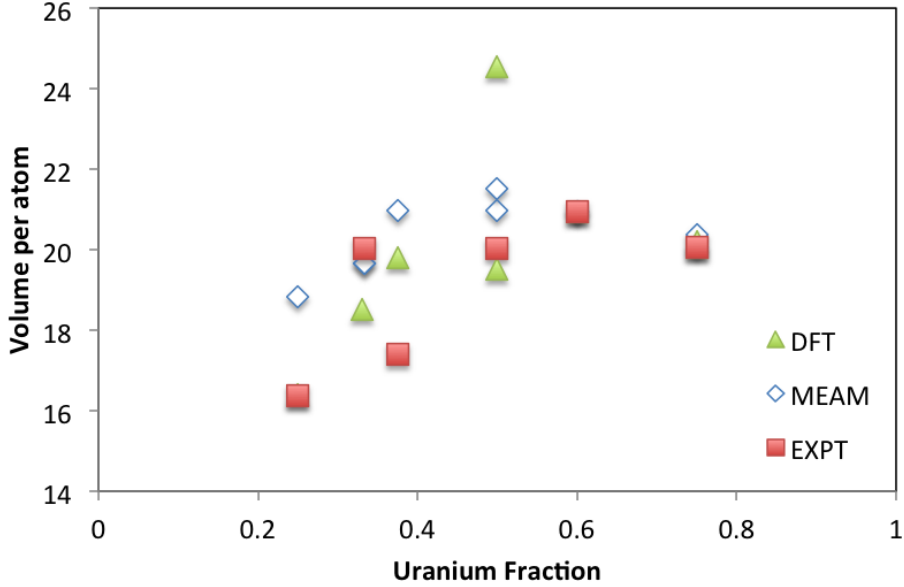


Figure 5: Volume per atom as a function of uranium concentration for a variety of phases in the U-Si system compared to DFT calculations [15] and experiments [13].

Although the ability to accurately predict the properties of a variety of crystal structures at 0 K is a critical step in the generation of a reasonable interatomic potential, being able to accurately model systems at non-zero temperatures is necessary to fully utilize the strength of molecular dynamics in branching the atomistic and mesoscopic time and length scales. Thus, the nature of  $\text{U}_3\text{Si}_2$  was examined as a function of temperature. A 360 atom ( $3 \times 3 \times 4$  unit cells) supercell is equilibrated at a given temperature in an NPT ensemble utilizing a Nose-Hoover barostat and a Langevin thermostat in the Grønbech-Jensen-Farago [47] formalism with a 1 fs timestep. The damping parameters for the Nose-Hoover barostat and the Langevin thermostat are 0.1 and 0.01, respectively. The target pressure is zero with the  $x$ ,  $y$  and  $z$  components independently controlled. The systems are equilibrated for 100 ps, with energies and volumes determined by averaging over the final 50 ps of the simulation. The total energy and total volume of the supercell as a function of temperature are displayed in figure 6. It is observed that the structure is stable and behaves predictably as a function of temperature. There are no observed obvious crystal structure changes or discontinuities suggesting potential instabilities. The structure was visually confirmed to be  $\text{U}_3\text{Si}_2$  throughout the temperature range investigated. The normalized lattice constants are also analyzed as a function of temperature to ensure there exist no structural irregularities. These are displayed in Figure 7. There is expansion of the  $a$  and  $b$  lattice constants in equal proportion as temperature increases, suggesting the tetragonal symmetry of the crystal structure is retained. The  $c$  lattice constant shows compression as temperature increases, and thus a decrease in the  $c/a$  ratio as temperature increases. The calculated MEAM average linear thermal expansion from 200 K to 1200 K is approximately  $15.8 \times 10^{-6} \text{ K}^{-1}$  and the experimental linear thermal expansion is  $14-17 \times 10^{-6} \text{ K}^{-1}$  from Shimizu [7] and  $16.1 \times 10^{-6} \text{ K}^{-1}$  from White [6]. This is remarkable agreement given that this was not

included into the fitting procedure. The molar heat capacity, given by equation 20, was calculated at 400 K for comparison with White, et al. [6]. The calculated value from the MEAM potential is 120.7 J/mol-K, which compares very favorably to the Dulong-Petit value of 125 J/mol-K and is slightly less than the experimental value of White, et al., which is 150 J/mol-K. It should be reiterated that this thermophysical property was not included into the fitting procedure, and thus this is considered excellent agreement to both theory and experiment. Regretfully, relatively little other experimental data exists for comparison.

$$C_P = \left( \frac{\delta H}{\delta T} \right)_P \quad (20)$$

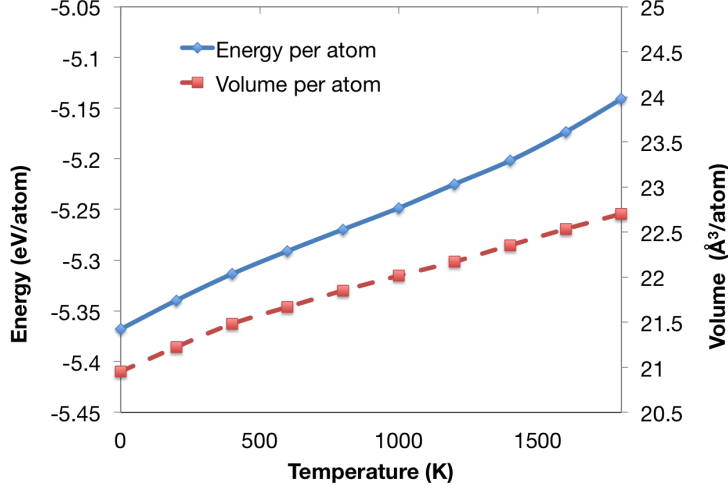


Figure 6: Energy per atom and volume per atom of  $\text{U}_3\text{Si}_2$  as a function of temperature

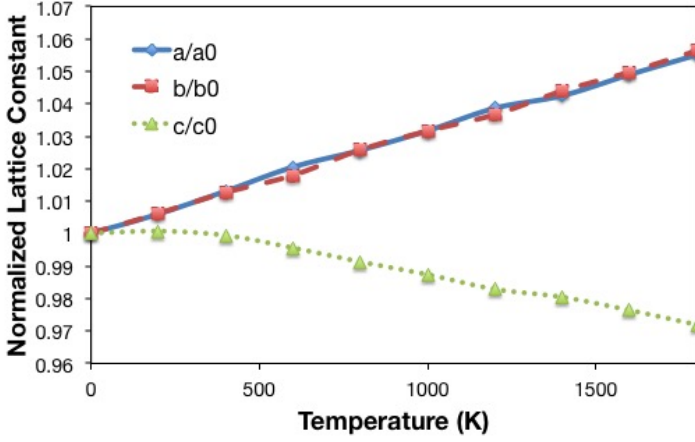


Figure 7: Variation of normalized lattice constants of  $\text{U}_3\text{Si}_2$  as a function of temperature.

As a nuclear fuel, it is necessary that this potential be able to model  $\text{U}_3\text{Si}_2$  under irradiation. In order to test the ability of the potential to model radiation damage, a 1 keV cascade is investigated. The

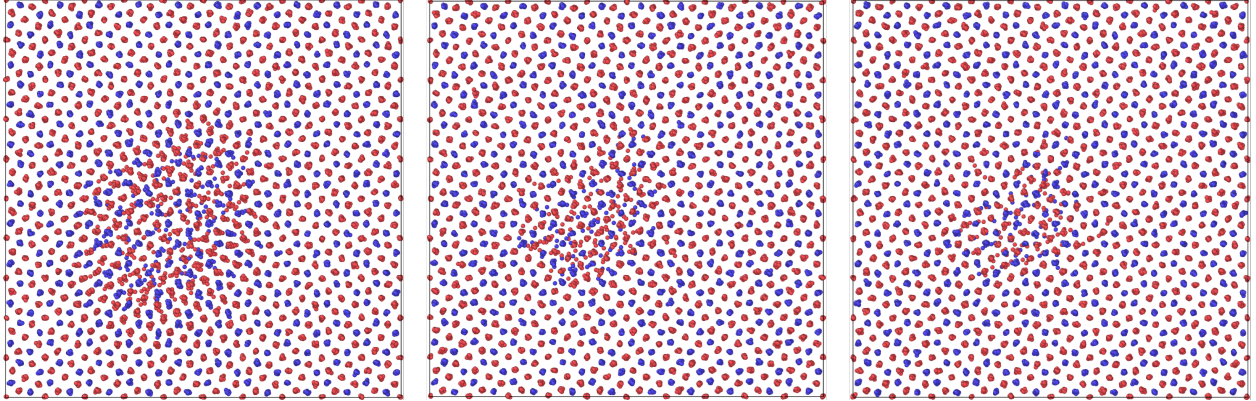


Figure 8: 1 keV cascade behavior of  $\text{U}_3\text{Si}_2$  at 500 K. The left-most panel is 0.4 ps after cascade initiation; the middle panel is 12 ps after cascade initiation; the right-most panel is 1 ns after cascade initiation.

MEAM potential is splined to a Ziegler-Biersack-Littmark (ZBL) [48] potential in the standardized method implemented into LAMMPS. A 20,000 atom supercell ( $10 \times 10 \times 20$  unit cells) is equilibrated at 500 K for 100 ps in an NPT ensemble with a target pressure of 0 GPa. In an NVT ensemble, a U1 atom is given additional kinetic energy in the [135] direction. The timestep is reduced to 0.2 fs and the cascade is allowed to evolve for 12 ps. The residual damage is then evolved at 500 K for 1 ns utilizing a 2 fs timestep. The state of the cascade and residual damage is displayed in Figure 8 at three different times throughout the simulation. It is observed that the crystal structure is stable and there exists a thermal spike and subsequent annealing stage. At 0.4 ps after cascade initiation, Wigner-Seitz analysis via Ovito [49] shows that there exist 68 Frenkel pairs; there exist 28 Frenkel pairs after 12 ps; there exist 17 Frenkel pairs after 1 ns. By investigating defects on each species sublattice, it can be determined the general nature of the defects generated via this specific cascade. Looking strictly at the uranium sublattice, 23 Frenkel pairs exist. Looking strictly at the silicon sublattice, 23 Frenkel pairs exist. This gives a total of 46 Frenkel pairs. It can thus be determined that in the total system there exist 28 Frenkel pairs and 18 anti-site defects, with the same number of defects on each sublattice. It can be concluded that this potential is displaying reasonable behavior under irradiation and the nature and number of defects can be readily determined. It should be noted that this is not intended to be a full radiation damage study, but simply an example that this potential produces reasonable radiation damage behavior. Radiation damage studies are certainly warranted in the future.

Another microstructural feature of interest is free surfaces. To ensure the potential is performing adequately with regards to surfaces, two systems are created to investigate both the (100) free surface and the (001) free surface (there exist multiple possible terminations, but in this work all terminuses are created at until cell boundaries). The system with free surfaces is equilibrated in an NPT ensemble at 500 K for 100 ps and the average energy is determined over the final 50 ps of the simulation. The relaxed structures of the (100) and (001) free surfaces are shown in Figure 9 and Figure 10, respectively. The first thing to notice is that the bulk structure remains stable and retains its crystal symmetry. There also exists some

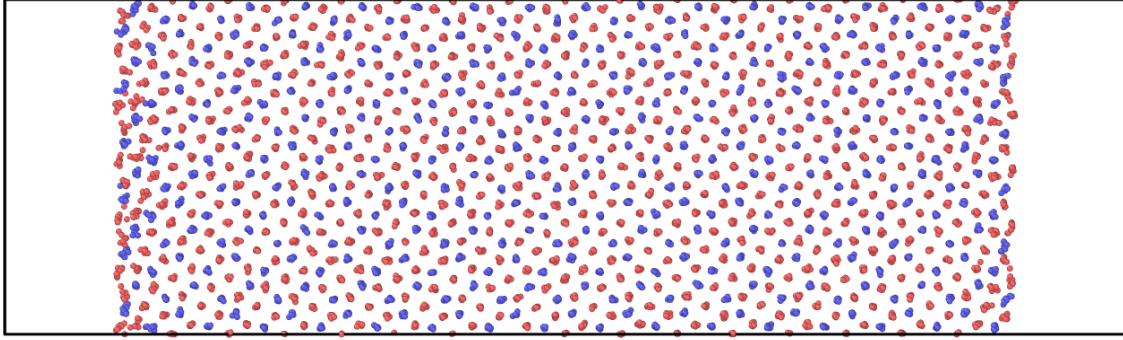


Figure 9: (100) free surface of  $\text{U}_3\text{Si}_2$  at 500 K after a 100 ps relaxation.

surface roughening along the first and second layers of atoms along the free surfaces. The surface energies are determined by equation 21

$$E_{surf} = \frac{(E^* - E)}{2 * A} * N \quad (21)$$

where  $E^*$  is the energy per atom of the system with two free surfaces,  $E$  is the energy per atom of the perfect crystal  $\text{U}_3\text{Si}_2$ ,  $A$  is the area of a free surface (multiplied by two because two free surfaces are present in the system) and  $N$  is the number of atoms in the system with two free surfaces. The resultant energy for the (100) surface is 0.99 J/m<sup>2</sup> and the (001) surface energy is 1.50 J/m<sup>2</sup>. A prior DFT study investigated free surfaces in  $\text{U}_3\text{Si}_2$  [50]. The surface energy was found to vary from 1.16 J/m<sup>2</sup> to 1.48 J/m<sup>2</sup>. The (100) surface has a surface energy of 1.48 J/m<sup>2</sup>, while the (001) surface has a surface energy of 1.43 J/m<sup>2</sup>. The nature of the lowest energy surface was not reported. Given that the physical nature of the surfaces as predicted by the MEAM potential is reasonable combined with the calculation of reasonable surface energies, it is suggested that the interatomic potential performs adequately for free surfaces in  $\text{U}_3\text{Si}_2$ . Of course, further experimental and computational investigations are required for validation of this predicted surface behavior. To further investigate the performance of the potential, a void is introduced into an equilibrated  $\text{U}_3\text{Si}_2$  system, and then further relaxed. It is observed that both voids of radius 4 Å (containing 13 vacancies) and 8 Å (containing 93 vacancies, shown in Figure 11) are stable within the structure up to 100 ps (when simulations were terminated). No void collapse is observed, no crystal structure collapse is observed, but minimal void surface reconstruction does occur. This further reinforces the suitability and stability of the potential for non-equilibrium systems.

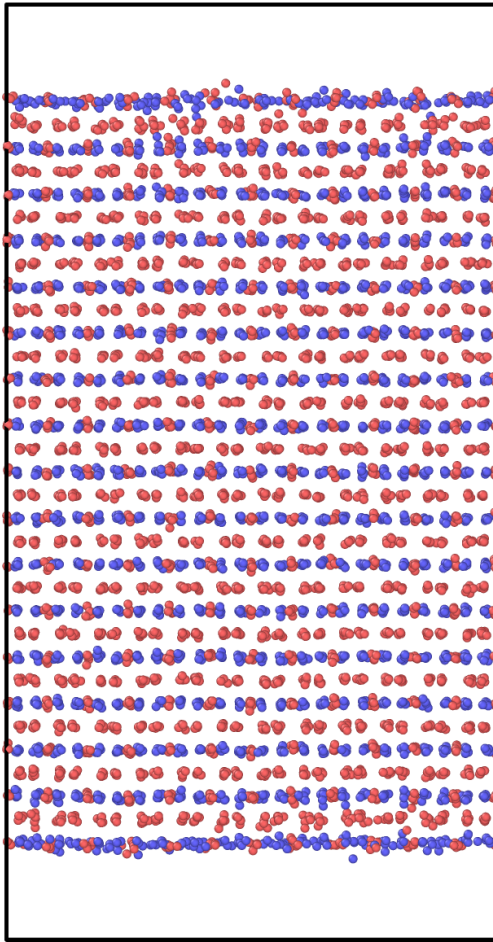


Figure 10: (001) free surface of  $\text{U}_3\text{Si}_2$  at 500 K after a 100 ps relaxation.

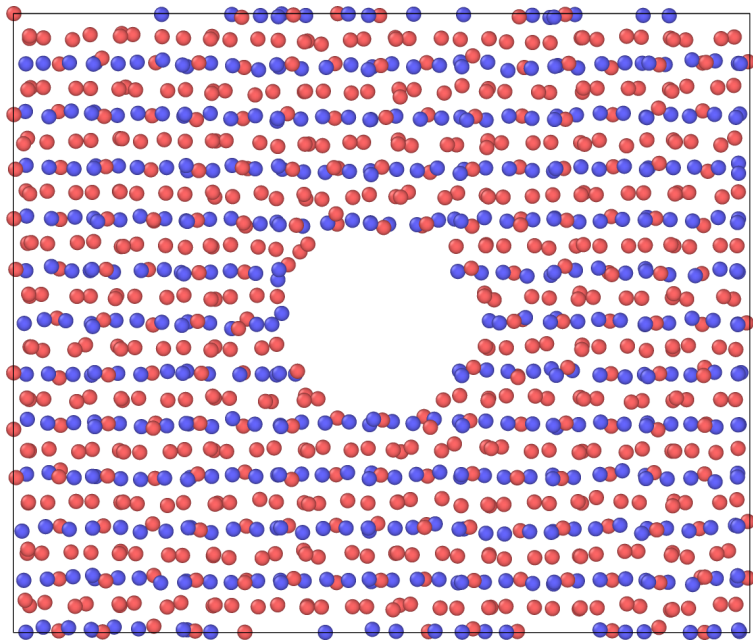


Figure 11: 2D projection of a 3D slice through the  $\text{U}_3\text{Si}_2$  supercell at 500 K containing a void with a radius of 8 Å.

## **5. Discussion**

The above assessment shows that the potential performs quite satisfactorily for the  $U_3Si_2$  phase with regards to cohesive energy, volume per atom, and elastic constants at 0 K, as well as the thermal expansion and heat capacity at non-zero temperatures. The potential is adequately sound in adjacent U-Si compounds, such as  $U_3Si$  and  $USi$ . The potential is not suited for describing low uranium content U-Si compounds, such as  $USi_3$ . Also, certain care needs to be exercised when investigating defects utilizing this potential, as important deviations from DFT calculations are observed. Finally, the potential is not intended for investigation of liquid phase  $U_3Si_2$ , as this was not taken into account in the fitting procedure nor fully explored by the authors.

Given the complex nature of the crystal structure of  $U_3Si_2$ , the inherent difficulties associated with the development of atomic potentials for pure uranium, let alone uranium-alloys, it is the opinion of the authors that a suitable interatomic potential to describe the U-Si system has been developed. Provided that the scientific community is continually gaining more knowledge on U-Si alloys via experimentation and first principles examinations, future refinement of the potential should be undertaken once more atomistic and fundamental property information has been gathered.

## **6. Conclusion**

A MEAM interatomic potential was developed for the U-Si system. The potential accurately describes 0 K properties of the primary phase of interest ( $U_3Si_2$ ), including formation energy, lattice constants, elastic constants and several point defect properties. The potential can also reasonably predict properties of a variety of U-Si phases across the composition spectrum. The predicted thermal expansion and heat capacity compare excellently to reported experimental values. The interatomic potential was tested by investigating the behavior of  $U_3Si_2$  under a 1 keV cascade, with free surfaces and in the presence of a void. The potential behaves in a reasonable manner in each of these three non-equilibrium cases. This potential can serve as a tool to branch experiments and recent first principles calculations to future longer time and larger length scale simulations.

## **7. Acknowledgments**

This work is supported by the U.S. Department of Energy, Office of Nuclear Energy, Nuclear Energy Advanced Modeling and Simulation (NEAMS) Accident Tolerant Fuel High-Impact-Problem Program. This manuscript has been authored by Battelle Energy Alliance, LLC under Contract No. DEAC07-05ID14517 with the U.S. Department of Energy. The United States Government retains and the publisher, by accepting the article for publication, acknowledges that the United States Government retains a nonexclusive, paid-up, irrevocable, world-wide license to publish or reproduce the published form of this manuscript, or allow others to do so, for United States Government purposes. Los Alamos National Laboratory, an affirmative

action/equal opportunity employer, is operated by Los Alamos National Security, LLC, for the National Nuclear Security Administration of the U.S. Department of Energy under Contract No. DE-AC52-06NA25396. This research made use of the resources of the High Performance Computing Center at Idaho National Laboratory, which is supported by the Office of Nuclear Energy of the U.S. Department of Energy and the Nuclear Science User Facilities under Contract No. DE-AC07-05ID14517.

## References

- [1] S. Zinkle, K. Terrani, L. Snead, Motivation for utilizing new high-performance advanced materials in nuclear energy systems, COSSMS 20 (2016) 401.
- [2] S. Zinkle, K. Terrani, J. Gehin, L. Ott, L. Snead, Accident tolerant fuels for lwr: A perspective, *J. Nucl. Mater.* 448 (2014) 374.
- [3] W. Zachariasen, Crystal chemical studies of the 5f-series of elements. viii. crystal structure studies of uranium silicides and of cesi<sub>2</sub>, npsi<sub>2</sub> and pusi<sub>2</sub>, *Acta Cryst.* 2 (1949) 94.
- [4] K. Remschnig, T. L. Bihan, H. Noel, P. Rogl, Structural chemistry and magnetic behavior of binary uranium silicides, *J. Solid. St. Chem.* 97 (1992) 391.
- [5] B. Massalski, *Binary Alloy Phase Diagrams*, second Ed., Materials Park, 1990, p. 3374.
- [6] J. White, A. Nelson, J. Dunwoody, D. Byler, D. Safarik, K. McClellan, Thermophysical properties of u<sub>3</sub>si<sub>2</sub> to 1773 k, *J. Nucl. Mater.* (2015) 275.
- [7] H. Shimizu, The properties and irradiation behavior of u<sub>3</sub>si<sub>2</sub>, Tech. Rep. NAA-SR-10621, Atomics International (1965).
- [8] S. Yagoubi, S. Heathman, A. Svane, G. Vaitheeswaran, P. Heines, J.-C. Griveau, T. L. Bihan, M. Idiri, F. Wastin, R. Caciuffo, High pressure studies on uranium and thorium silicide compounds: Experiment and theory, *J. Alloys and Compounds* 546 (2013) 63.
- [9] P. Gross, C. Hayman, H. Clayton, Thermodynamics of nuclear materials, IAEA (1962) 653.
- [10] P. O'Hare, et. al., Thermodynamics of nuclear materials, IAE Vienne 2 (439).
- [11] C. Alcock, P. Grievson, A thermodynamic study of the compounds of uranium with silicon, germanium, tin, and lead, *J. Inst. Metals* 90 (1962) 304.
- [12] M. Rand, O. Kubaschewski, *The Thermochemical Properties of Uranium Compounds*, Oliver and Boyd, 1963, p. 46.
- [13] A. Berche, C. Rado, O. Rapaud, C. Gueneau, J. Rogez, Thermodynamic study of the u-si system, *J. Nucl. Mater.* 389 (2009) 101.

- [14] M. Finlay, G. Hofman, J. Rest, J. Snelgrove, Behavior of irradiated uranium silicide fuel revisited, Tech. rep., International Meeting on RERTRs (2002).
- [15] M. Noordhoek, T. Besman, D. Andersson, S. Middleburgh, A. Chernatynskiy, Phase equilibria in the u-si system from first-principles calculations, *J. Nucl. Mater.* 479 (2016) 216–223.
- [16] B. Beeler, C. Deo, M. Baskes, M. Okuniewski, Atomistic properties of gamma uranium, *J. Phys.: Cond. Mat.* 24 (2012) 075401.
- [17] B. Beeler, C. Deo, M. Baskes, M. Okuniewski, Atomistic investigations of intrinsic and extrinsic point defects in bcc uranium, *Effects of Radiation on Nuclear Materials: STP 1547* 25 (2012) 231.
- [18] J. Fernandez, M. Pascuet, On the accurate description of uranium metallic phases: a meam interatomic potential approach, *Modelling Simul. Mater. Sci. Eng.* 22 (2014) 055019.
- [19] R.-S. Li, B. He, Q.-H. Zhang, Atomistic model of uranium, *Chin. J. Chem. Phys.* 24 (2011) 405.
- [20] D. Smirnova, S. Starikov, V. Stegailov, Interatomic potential for uranium in a wide range of pressures and temperatures, *J. Phys.: Cond. Mat.* 24 (2012) 149501.
- [21] Y. Li, T. Shan, T. Liang, S. Sinnott, S. Phillpot, Classical interatomic potential for orthorhombic uranium, *J. Phys.: Cond. Mat.* 24 (2012) 235403.
- [22] A. Moore, B. Beeler, C. Deo, M. Baskes, M. Okuniewski, Atomistic modeling of high temperature uranium-zirconium alloy structure and thermodynamics, *J. Nucl. Mater.* 467 (2015) 802.
- [23] M. Pascuet, G. Bonny, J. Fernandez, Many-body interatomic u and al-u potentials, *J. Nucl. Mater.* 424 (2012) 158.
- [24] D. Smirnova, A. Kuksin, S. Starikov, V. Stegailov, Z. Insepov, J. Rest, A. Yacout, A ternary eam interatomic potential for u-mo alloys with xenon, *Modelling Simul. Mater. Sci. Eng.* 21 (2013) 035011.
- [25] M. Daw, M. Baskes, Embedded-atom method - derivation and application to impurities, surfaces, and other defects in metals, *Phys. Rev. B* 29 (1984) 6443.
- [26] M. Daw, S. Foiles, M. Baskes, The embedded-atom method: a review of theory and applications, *Mat. Sci. Rep.* 9 (1993) 251–310.
- [27] M. Daw, M. Baskes, Semiempirical, quantum mechanical calculation of hydrogen embrittlement in metals, *Phys. Rev. Lett.* 50 (1983) 1285.
- [28] P. Olsson, Semi-empirical atomistic study of point defect properties in bcc transition metals, *Comp. Mat. Sci.* 47 (2009) 135.

- [29] D. Belaschenko, D. Smirnova, Modeling the molecular dynamics of liquid metals at high pressures: Liquid potassium, *Russ. J. Phys. Chem.* 85 (2011) 1908.
- [30] X. Liu, H. Liu, J. Dong, X. Xie, Molecular dynamics simulation on phosphorus behavior at ni grain boundary, *Scripta Materialia* 42 (1999) 189.
- [31] M. Chassange, M. Legros, D. Rodney, Atomic-scale simulation of screw dislocation/coherent twin boundary interaction in al, au, cu and ni, *Acta mater.* 59 (2011) 1456.
- [32] G. Li, Q. Wang, D. Li, J. He, Size and composition effects on the melting of bimetallic cu-ni clusters studied via molecular dynamics simulation, *Mater. Chem. Phys.* 114 (2009) 746.
- [33] I. Vatne, E. Ostby, C. Thaulow, D. Farkas, Multiscale simulations of mixed-mode fracture in bcc-fe, *Mat. Sci. Eng. A* 528 (2011) 5122.
- [34] J. Rose, J. Smith, F. Guinea, J. Ferrante, Universal features of the equation of state of metals, *Phys. Rev. B* 29 (1984) 2963.
- [35] M. Baskes, Modified embedded-atom potentials for cubic materials and impurities, *Phys. Rev. B* 46 (1992) 2727.
- [36] M. Baskes, Atomistic model of plutonium, *Phys. Rev. B* 62 (2000) 15532.
- [37] M. Baskes, Application of the embedded-atom method to covalent materials: A semiempirical potential for silicon, *Phys. Rev. Lett.* 59 (1987) 2666.
- [38] M. Baskes, J. Nelson, A. Wright, Semiempirical modified embedded-atom potentials for silicon and germanium, *Phys. Rev. B* 40 (1989) 6085.
- [39] S. Valone, M. Baskes, R. Martin, Atomistic model of helium bubbles in gallium-stabilized plutonium, *Phys. Rev. B* 73 (2006) 214209.
- [40] R. Ravelo, M. Baskes, Equilibrium and thermodynamic properties of grey, white, and liquid tin, *Phys. Rev. Lett.* 79 (1997) 2482.
- [41] S. Nouraniuan, M. Tschopp, S. Gwaltney, M. Baskes, M. Horstemeyer, An interatomic potential for saturated hydrocarbons based on the modified embedded-atom method, *Phys. Chem. Chem. Phys.* 16 (2014) 6233.
- [42] K. Huber, G. Herzberg, *Constants of Diatomic Molecules*, Van Nostrand, 1979.
- [43] S. Plimpton, Fast parallel algorithms for short-range molecular dynamics, *J. Comp. Phys.* 117 (1995) 1–19.
- [44] M. Cohen, Calculation of bulk moduli of diamond and zinc-blend solids, *Phys. Rev. B* 32 (1985) 7988.

- [45] F. Birch, Finite elastic strain of cubic crystals, *Phys. Rev.* 71 (1947) 809.
- [46] S. Middleburgh, R. Grimes, E. Lahoda, C. Stanek, D. Andersson, Non-stoichiometry in u3si2, *J. Nucl. Mater.* 482 (2016) 300.
- [47] N. Gronbech-Jensen, O. Farago, A simple and effective verlet-type algorithm for simulating langevin dynamics, *Mol. Phys.* 111 (2013) 983.
- [48] J. Ziegler, J. Biersack, U. Littmark, *Stopping and Ranges of Ions in Matter*, Pergamon Press, 1985.
- [49] A. Stukowski, Visualization and analysis of atomis simulation data with ovito - the open visulaization tool, *Modeling and Simulation of Materials Science and Engineering* 18 (2010) 015012.
- [50] Y. Miao, B. Ye, G. Hofman, A. Yacout, K. Gamble, Z.-G. Mei, Rate theory modeling and simulation of silicide fuel at lwr conditions, *Tech. rep.*, ANL/NE-16/13 130024 (2016).